Computational and Theoretical Chemistry 1078 (2016) 1–8

Contents lists available at ScienceDirect

Computational and Theoretical Chemistry

journal homepage: www.elsevier.com/locate/comptc

The origin of the stereoselective alkylation of 3-substituted-2-oxopiperazines: A computational investigation

Christine Cézard *, Benjamin Bouvier, Alexandra Dassonville-Klimpt, Pascal Sonnet

Laboratoire de Glycochimie, des Antimicrobiens et des Agroressources (LG2A) – CNRS FRE 3517, UFR de Pharmacie, Université de Picardie – Jules Verne, 1 Rue des Louvels, 87037 Amiens Cedex 1, France

ARTICLE INFO

Article history:
Received 20 October 2015
Received in revised form 9 December 2015
Accepted 10 December 2015
Available online 31 December 2015

Keywords:
2-Oxopiperazine
Alkylation
DFT calculations
Transition states
Reaction path
Stereospecificity

ABSTRACT

2-Oxopiperazines and their derivatives are important pharmacophores found in numerous bioactive products. The potency of these compounds depends on the nature and/or position of their substituent (s) as well as on their chirality. Hence, it is important to develop, control and optimize synthetic routes leading to enantiomerically pure substituted 2-oxopiperazines. In this work we report on the origin of this stereoselectivity, upon alkylation of 2-oxopiperazines at position C_3, studied by means of quantum chemistry calculations. Indeed, this alkylation with methyl chloride is predicted to afford mainly the *exo* product with a 98:2 ratio. To this purpose, we model the reaction path leading to both enantiomers by scrutinizing the structures and energetics of the pre-reaction complexes, the transition states and the post-reaction complexes. The computational results are in good agreement with the experimental observations, and provide valuable insights into the origins of this specificity. From the conformational analysis of the piperazine ring and of intramolecular interaction patterns, we show that the enantiofacial discrimination is achieved by a subtle balance between sterical hindrance and control of the conformation of the piperazine ring.

1. Introduction

Piperazines, symmetrical cyclic 6-ring molecules containing four carbon atoms and two nitrogen atoms at opposing position (see Fig. 1a), represent a broad class of chemical compounds with many pharmacological properties and applications. Molecules featuring a piperazine scaffold have been reported to have diverse biological activities (antihistaminic, antihelmintic, anticancer, antidepressant, antifungal, antibacterial, ...) depending on their substitution [1–9]. Indeed, piperazines can be substituted at nitrogen or carbon atoms, conferring the newly formed molecule with specific activities. For instance, simple *N*-substituted piperazines can be found in numerous drugs and/or recreational drugs [10]. While substituting a piperazine on a nitrogen atom remains rather easy, a stereo-controlled substitution on a carbon position remains quite a challenge to organic chemists. Methods used for the preparation of asymmetric substituted piperazines include enantioselective hydrogenation [11], stereoselective alkylation of 2-oxopiperazines using a chiral auxiliary [12–17], α-lithiation mediated by chiral ligands such as (−)-sparteine [18,19] or synthesis from a chiral pool of compounds such as naturally occurring amino acids [20–23]. Nowadays, because of numerous recurrent positive hits in screenings, piperazine derivatives and especially their keto analogues are considered as important and privileged scaffolds in medicinal chemistry [24]. In this paper, we will focus on 2-oxopiperazines (or piperazin-2-ones, i.e., piperazines featuring a carbonyl function at position 2, see Fig. 1b) and their chiral syntheses and/or substitutions. Although less frequently employed in pharmaceutical chemistry, oxopiperazines [25] are important pharmacophores particularly found in bioactive drugs used in central nervous system therapies [26], used to mimic inverse γ-turns in peptides [27], or as efficient chiral ligands in enantioselective catalysis [28]. Rhodotorulic acid (*N*-[3-[5-[3-[acetyl(hydroxy)amino]propyl]-3,6-dioxopiperazin-2-yl]propyl]-*N*-hydroxyacetamide, see Fig. 1c), for instance, a natural iron chelator produced by *Rhodotorula pilimanae* [29], features two asymmetric centers at position 3 and 6 with identical configurations. Swapping of one of those chiralities impacts the formation (rate and spatial arrangement) of the corresponding iron complexes [30,31]. Hence, when considering 2-oxopiperazine derivatives, it is of paramount importance to master enantioselective synthesis routes, as the presence and chirality of substituents at the different positions of the piperazine heterocycle have a direct and significant influence on the biological activity.

Our group is specialized in asymmetric substitution of 2-oxopiperazines at various C-positions and stereosynthesis of

* Corresponding author.
E-mail address: christine.cezard@u-picardie.fr (C. Cézard).

http://dx.doi.org/10.1016/j.comptc.2015.12.005
2210-271X/

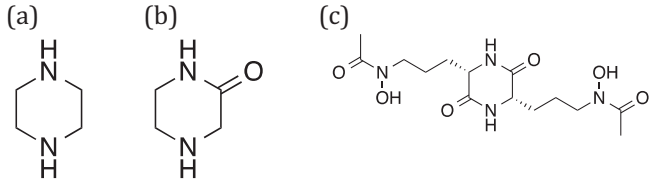

Fig. 1. Structure of a piperazine (a), a 2-oxopiperazine (b) and rhodotorulic acid (c).

polysubstituted oxopiperazines [32,33]. We have, in particular, proposed a new pathway to chiral 3-substituted-2-oxopiperazines based on a stereoselective alkylation of 1,4-disubstitu ted-2-oxopiperazines with different electrophiles (BnBr, CH_3Cl, ...) by using a chiral alcohol inductor grafted to N_1 (Scheme 1). While such syntheses are now routine and afford C_3-1,4-disubstitu ted-2-oxopiperazines with high yields and diastereomeric excesses (>96%), the mechanisms underlying this stereospecificity are still unclear. To address this shortcoming, we study the C_3-alkylation of 1,4-disubstituted-piperazin-2-one (1′*R*)-**1** using quantum chemical methods. To alleviate the cost of accurate calculations on these molecules, we use methyl chloride as a model electrophile (Scheme 2). We focus on the impact of (i) reaction energetics, (ii) transition states structures and (iii) reaction paths on alkylation stereospecificity. Similar studies have already been performed on piperidine [34–36] and piperidone [37] derivatives but to the best of our knowledge, no such studies have ever been performed on oxopiperazine derivatives.

2. Methods

2.1. Models

We wish to make it clear that the species chosen as targets of our computational study may not correspond to the actual reactive intermediates present in solution and described in Scheme 1. Upon addition of a strong base such as LDA on reactant **1** in THF, deprotonation of both the hydroxyl function and position C_3 will likely occur; the reactive species thus formed would present two anionic sites, which would subsequently be chelated by lithium. The hydroxyl function, being more acidic, is deprotonated before the C_3 position and thereby binds lithium first. Micouin et al. proposed a potential mechanism involving a transition state featuring two lithium cations to explain the *exo* preference of the reaction [38]. Modeling the reactive species using two anionic sites or chelated by two lithium cations did not seem desirable as the incoming methyl chloride and/or the Li^+ would not be able to discriminate between the two reactive sites and consequently either aggregate or repulse one another. Moreover, it is known that lithium conjugates used in organic synthesis (organolithium reagents, lithium enolates, ...) form oligomers that can only achieve sufficient stabilization *via* interactions with other molecules that help fulfill the octet rule on lithium [39,40] (e.g., solvents such as THF); yet the choice of the number of solvent molecules to explicitly include in quantum chemistry calculations, as well as their placement around lithium, raise difficult practicality issues. Hence, as a first step toward the understanding of the stereospecificity of the reaction, we have chosen not to introduce lithium (whether in form of single ions or aggregated with THF molecules) in our initial model, but to retain the hydroxyl group in the reactant. This simplified model provides a cost-effective approximation of the actual reactive species, considering that the hydrogen atom belongs to the first group of the periodic table. Nevertheless, it has been suggested [38,41] that in such systems, coordination with a Li^+ cation may be the key factor in the stereospecificity; to ascertain whether this is the case, we performed an additional series of calculations with an actual lithium atom (in place of the hydroxyl hydrogen) bridging the two anionic sites together. The presence of the second lithium atom in the calculations is not mandatory, as it does not influence the stereoselectivity. This fact was demonstrated by a

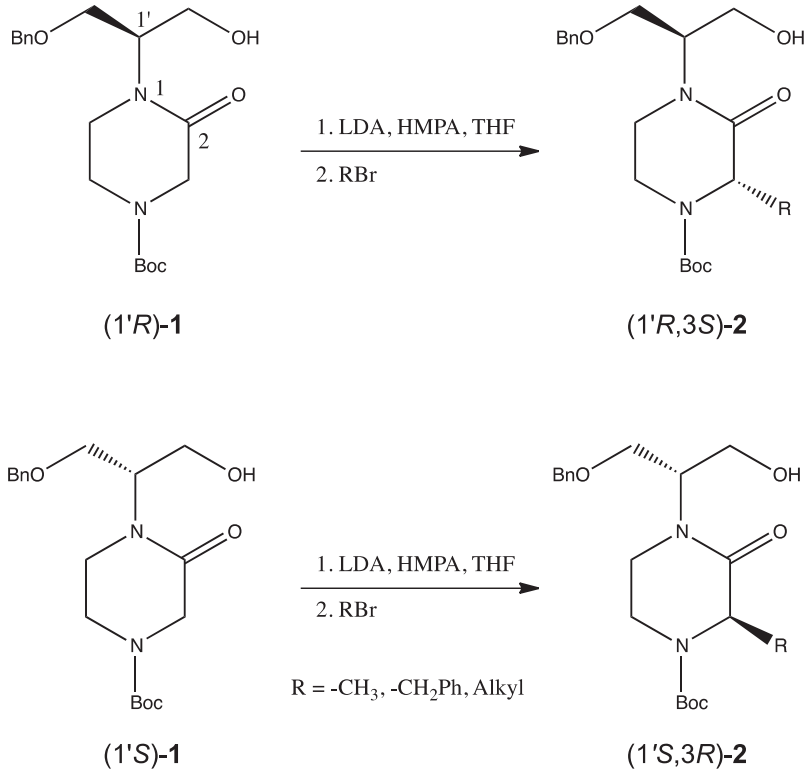

(1′*R*)-**1** (1′*R*,3*S*)-**2**

(1′*S*)-**1** (1′*S*,3*R*)-**2**

Scheme 1. Alkylation of 2-oxopiperazine (1′*R*)-**1** and (1′*S*)-**1**.

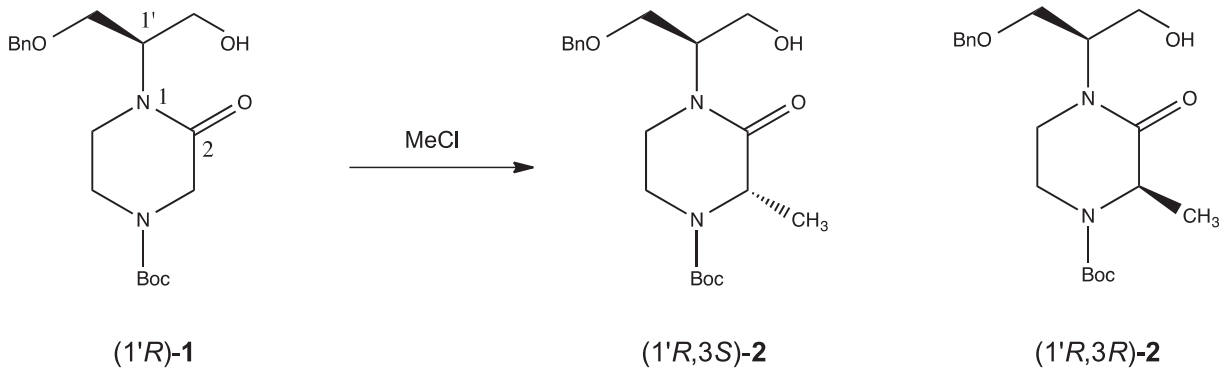

Scheme 2.

series of experiments [42] and by theoretical studies [37] on systems featuring one negatively charged oxygen.

3. Computational details

All calculations were performed using the Gaussian 09 program [43]. Full geometry optimizations were performed in the gas phase with the hybrid B3LYP density functional method [44–46] using the 6-31+G* basis set, which represents a good compromise between accuracy and computational cost. Indeed, considering the large size of the systems, using higher-level methods for full optimization would not have been cost-effective. When mentioned, single point MP2/6-31+G* calculations were subsequently undertaken to determine the relative energies of the different products formed during the alkylation reactions. Frequency calculations were performed to verify the true nature of stationary points. Vibrational frequency calculations gave only one imaginary frequency for all transition structures, confirming their saddle-point nature, whereas all other structures were verified as minima with all-positive frequency values. Zero-point, thermal and entropic corrections at a pressure of 1 atm and a temperature of 195 K (unless otherwise specified) were added to the electronic energies to calculate the Gibbs free energies in the gas phase. Basis Superposition Set Errors (BSSE) can be neglected in calculations of such systems as discussed in Refs. [35,37]. Intrinsic Reaction Coordinate analyses have been conducted to obtain the pre-reaction and post-reaction complexes connected to a transition state. The quantum theory of atoms in molecules (QTAIM) derived data were calculated with the Multiwfn software [47].

To estimate the influence of solvation, SCRF continuum calculations were performed at the B3LYP/6-31+G* level of theory. Calculations were performed in water (ε = 78.3553), *n*-octanol (ε = 9.8629), tetrahydrofuran (ε = 7.4257), chloroform (ε = 4.7113) and carbontetrachloride (ε = 2.2280) to estimate the effect of the increasing polarity of the solvent.

4. Results and discussion

The stereoselectivity of the alkylation in position 3 of 2-oxopiperazine (1′*R*)-**1** was examined. To this purpose, the reaction of the enolate derived from (1′*R*)-**1** with methyl chloride as the electrophile was investigated (see Scheme 1) in the gas phase as well as in solution. In a first step, conformational searches of the different reactants ((1′*R*)-**1** and the enolate derived from (1′*R*)-**1**) and products ((1′*R*,3*S*)-**2** *exo* and (1′*R*,3R)-**2** *endo*) have been performed in the gas phase, which led to two representative families of isomers, located within a range of 10 kcal mol^{-1} and showing different intramolecular hydrogen bonding patterns involving the hydroxyl function of the piperazine ring (see Fig. 2), namely HB-1 and HB-2. HB-1 refers to the interaction between —OH and the carbonyl function —C=O of the piperazine ring, whereas HB-2 refers to the interaction between —OH and the ether function —C—O—C— of the —OBn group.

While the most stable structure for (1′*R*)-**1** is based on pattern HB-2, the HB-1 pattern is found in the most stable structures for the enolate and both the products. The free energy differences G (HB-1) – G(HB-2) in the gas phase are +0.5, −8.1, −2.0 and −0.6 for (1′*R*)-**1**, the enolate of (1′*R*)-**1**, the *exo* product and the *endo* product, respectively. It has to be acknowledged that the position/direction of the OBn substituent does not alter the global stability as many conformers differing only by the OBn position lie within less than 1 kcal mol^{-1}.

Energy and free energy differences when considering the most stable structure of each compound (reactant: enolate from (1′*R*)-**1** and products (1′*R*,3*S*)-**2** and (1′*R*,3*R*)-**2**) are reported in Table 1. These results indicate that the ((1′*R*,3*S*)-**2**, i.e., *exo*) product is always favored, independently of the calculation method used. B3LYP and MP2 methods provide comparable results when considering the gas phase, but the latter predicts a slighter stabilization of the *exo* product in solvent. Solvation free energies are of the same magnitude than that in the gas phase, indicating that stereoselectivity is unaffected by the polarity of the solvent. Experimentally, the (1′*R*,3*S*)-**2**:(1′*R*,3*R*)-**2** ratio is at least 98:2 [32,33], which implies a free energy difference of at least 1.5 kcal mol^{-1} under experimental conditions (1 atm, −78 °C).

In order to investigate the influence of kinetic effects in the stereoselective alkylation of (1′*R*)-**1**, the free energies of the transition states and their respective pre- and post-reaction (abbreviated as PreRC and PostRC, respectively in the remainder of the text)

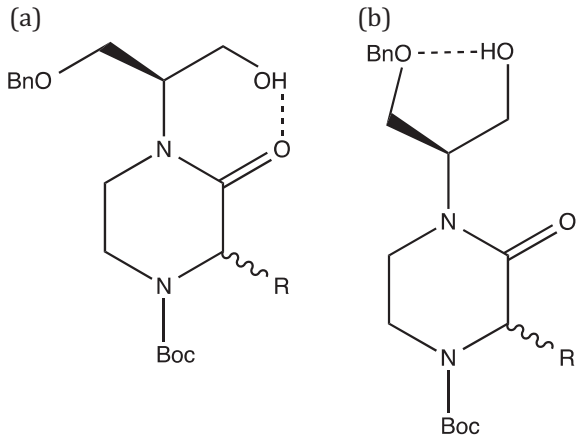

Fig. 2. Intramolecular hydrogen bonding patterns. (a) HB-1 and (b) HB-2.

Table 1
Energy and free energy differences (in kcal mol^{-1}) of separated products computed at the B3LYP/6-31+G* and MP2/6-31+G* levels of theory at a temperature of 298 K and a pressure of 1 atm. ΔE energies are ZPE corrected.

	Gas phase		CCl_4	$CHCl_3$	THF	*n*-Octanol	Water
	$\Delta(E+ZPE)$	ΔG	ΔG	ΔG	ΔG	ΔG	ΔG
*B3LYP/6-31+G**							
2 *exo*	−33.6	−29.2	−45.3	−50.6	−51.9	−52.5	−53.1
3 *endo*	−31.5	−27.3	−43.9	−48.8	−50.3	−51.0	−51.7
Δ	2.1	1.9	1.4	1.8	1.6	1.5	1.4
*MP2/6-31+G**							
2 *exo*	−39.8	−33.4	−55.9	−50.5	−57.4	−58.0	−59.4
3 *endo*	−37.5	−31.6	−54.0	−48.7	−55.5	−56.1	−57.4
Δ	2.3	1.8	1.9	1.8	1.9	1.9	2.0

complexes have to be evaluated. In principle, many conformations should be considered, but as previously mentioned, conformational searches of the free enolate followed by clustering generated two main families of structures differing by the nature of their intramolecular hydrogen bond. Within these families, two subgroups emerged according to the conformation of the piperazine ring and the position of the —OBn substituent, hence eight different enol conformations. Representative geometries of the two families with their sub-structures are represented in Figs. SI1 and SI2 along with their relative energies. The transition structures for both *exo* and *endo* attacks of methyl chloride based on these eight families of conformers were located and in all cases the *exo* TS were more stable than the *endo* ones. The most stable enols for each families present an additional stabilization due to an interaction with the —OBn group. However, it is interesting to note that, depending on the intramolecular HB pattern considered, the most stable enols do not present the same piperazine cycle conformation. Hence, based on these considerations, we have selected two structural matching structures (one from each HB family) that seemed the most appropriate from a chemical point of view, featuring: (i) a "free" —OBn moiety, so as to avoid interaction with the reactive site and not to favor one attack over the other because of obvious steric hindrance upon approach of the methyl chloride and (ii) the HB-1 conformation of the piperazine cycle. Subsequently, starting from these two enols, transition structures (TS) for both *exo* and *endo* attacks of methyl chloride were located and the optimized structures of both the pre-reaction and post-reaction complexes were obtained from IRC calculations.

In the remainder of the text, we will focus on two reaction paths (RP):

(i) RP1 involving structures featuring the HB-1 intramolecular hydrogen bond, i.e., the interaction between the alcohol function —OH and the carbonyl function —C=O of the piperazine ring (see Table 2 as well as Figs. 3 and SI3–5 featuring the structures and energies of PreRC1, TS1 and PostRC1).
(ii) RP2 involving structures featuring the HB-2 intramolecular hydrogen bond, i.e., the interaction between the alcohol function —OH and the ether function —C—O—C— of the —OBn group (see Table 3 as well as Figs. 4 and SI6–8 representing the structures and energies of PreRC2, TS2 and PostRC2).

4.1. Pre-reaction complexes (PreRC)

First of all, it has to be acknowledged that the energy difference between the *exo* structures of PreRC1 and PreRC2 is in favor of PreRC1 by 5.6 kcal mol^{-1}. Depending on the intramolecular hydrogen bonding pattern considered, the pre-reaction complexes leading to the *endo* (1′*R*,3*R*)-**2** and *exo* (1′*R*,3*S*)-**2** products do not

Table 2
Free energy differences (in kcal mol^{-1}) at a temperature of 195 K and a pressure of 1 atm of Pre-Reaction complexes, Transition States and Post-Reaction complexes for RP1 in the gas phase and in solution.

Solvent	Approach	Pre-RC	TS	Post-RC
Gas phase	*exo*	0.0	10.3	−45.0
	endo	1.4	12.7	−40.0
CCl_4	*exo*	0.0	7.4	−49.7
	endo	0.2	9.4	−46.1
$CHCl_3$	*exo*	0.0	8.6	−50.1
	endo	0.6	9.4	−49.0
THF	*exo*	0.0	8.5	−50.4
	endo	0.8	9.0	−49.8
n-Octanol	*exo*	0.0	8.5	−50.5
	endo	0.9	8.7	−50.3
Water	*exo*	0.1	7.5	−52.0
	endo	0.0	8.5	−51.5

present similar free energy stabilities. While the two conformations show similar energies for HB-2 with a methyl chloride adopting a quite symmetrical position for both attacks, a difference of 1.4 kcal mol^{-1} is observed for HB-1 in favor of the *exo* approach. Indeed the position of the OH···O hydrogen bond influences the *endo* ingress of the methyl chloride. Although the C_M—C_3 distance is shorter for the *endo* approach (3.51 Å *vs.* 3.62 Å), the C—H···O interaction between the carbonyl oxygen and one of the hydrogen atoms of the methyl chloride is much weaker (3.86 Å *vs.* 2.17 Å). Such a short distance is indicative of the existence of a bond path linking the two atoms, which was indeed confirmed in the *exo* complex with an electron density ρ_{bcp} = 0.0181 au at bond critical point. No such path was identified in the *endo* complex. These interactions and values are in agreement with those of Soteras et al. while studying the alkylation of oxazolopiperidones [37]. In RP2, by construction, the incoming of the methyl chloride is not impeded by the presence of the intramolecular hydrogen bond, hence the similar positions of the methyl chloride and the similar energies. The C—H···O distances between the carbonyl oxygen and one of the hydrogen atoms of the methyl chloride are 2.13 Å and 2.17 Å for *exo* and *endo*, respectively. The densities at bond critical point are 0.0196 au and 0.0180 au for *exo* and *endo*, respectively attesting to the presence of a bond path in both attacks. It has to be acknowledged that in both RPs the overall structure of the enols are nearly superimposable for the two attacks, their rmsd being 0.3 Å and 0.1 Å for PreRC1 and PreRC2, respectively.

4.2. Transition state (TS)

For both reaction paths considered, the transition state leading to the *exo* product is favored (by 2.4 kcal mol^{-1} for TS1 and by 0.8 kcal mol^{-1} for TS2), although (i) the C_M—C_3 distances are shorter for the two *endo* attacks and (ii) the positions of the incoming methyl chloride are only slightly nonsymmetrical for both attacks. In TS1, the C_M—C_3 distances are 2.38 Å and 2.37 Å for the *exo* and *endo* approaches, respectively. The *endo* attack leads to a less eclipsed position of the incoming methyl chloride (C_M—C_3—C_2—O dihedral angle of 77° and 75°, for *exo* and *endo*, respectively) because of sterical hindrances with the axial hydrogen of C_6 and the alcohol function involved in HB-1, resulting in a weaker C—H···O interaction (2.93 Å *vs.* 2.76 Å for *exo*), a deformation of the piperazine cycle and a spatial rearrangement of HB-1, hence a destabilization. Indeed, the formation of the *endo* TS is impeded by the presence of the axial hydrogen of C_6, with a H···H distance of 2.33 Å, which is smaller than two times the van der Waals radius of hydrogen (r_H = 1.2 Å). In TS2, by construction, only the steric hindrance with the axial hydrogen of C_6 might remain. While the

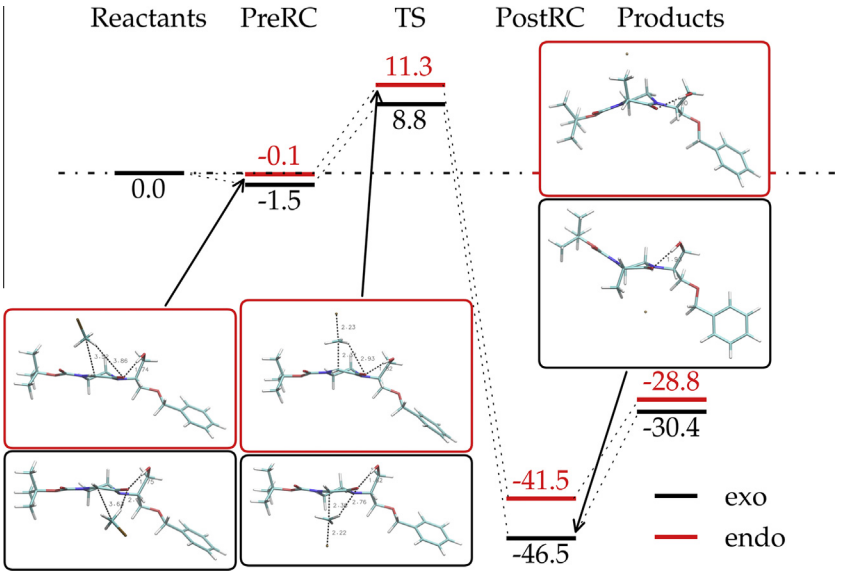

Fig. 3. Pre-reaction (PreRC), transition state (TS) and post-reaction (PostRC) structures for the *exo* and *endo* attacks of the HB-1 intramolecular hydrogen-bonded enolate of (1′R)-**1** by methyl chloride. The free energy differences between each state and the reactants are given in kcal mol^{-1}. Better quality images of the structures are given in Supplementary Information (SI3–5).

Table 3
Free energy differences (in kcal mol^{-1}) at a temperature of 195 K and a pressure of 1 atm of Pre-Reaction complexes, Transition States and Post-Reaction complexes for RP2 in the gas phase and in solution.

Solvent	Approach	Pre-RC	TS	Post-RC
Gas phase	*exo*	0.0	7.6	−53.2
	endo	0.0	8.4	−47.6
CCl_4	*exo*	0.0	5.1	−56.1
	endo	0.7	5.7	−52.9
$CHCl_3$	*exo*	0.0	5.9	−55.5
	endo	1.0	7.0	−53.5
THF	*exo*	0.0	7.2	−55.2
	endo	1.2	7.1	−53.5
n-Octanol	*exo*	0.6	6.1	−56.2
	endo	0.0	6.0	−54.5
Water	*exo*	0.0	5.6	−57.2
	endo	0.3	5.2	−55.9

methyl chloride is less attracted by the 2-oxopiperazine in the HB-2 conformation (the C_M—C_3 and C—H···O distances are longer than in the HB-1 structures), there is no relevant difference in its location between the two attacks as there is no specific steric interaction in the TS2 transition structures. The main difference between the two structures is the value of the O—C_2—C_3—H dihedral angle, which is 25° and 20° for the *exo* and *endo* attacks respectively, attesting to slight non-equivalent torsional strains in the piperazine cycle upon alkylation at the C_3 position. Consequently, the *exo* and *endo* TS2 are less than 1 kcal mol^{-1} apart. The *exo* and *endo* structures of the "TS enol" show different deformations as confirmed by a rmsd of 0.56 Å and 0.25 Å, respectively. It has to be acknowledged that the energy difference between the *exo* structures of TS1 and TS2 is of 2.9 kcal mol^{-1} in favor of TS1 in the gas phase.

4.3. Post-Reaction Complexes (PostRC)

For both hydrogen patterns the product obtained through the *exo* attack is clearly favored and is around 5 kcal mol^{-1} more stable (5.0 kcal mol^{-1} for HB-1 and 5.6 kcal mol^{-1} for HB-2, see Tables 2 and 3). The *exo* attacks lead to (1′*R*,3*S*)-**2** products with an equatorial —CH_3 at the C_3 position, while *endo* attacks lead to (1′*R*,3*R*)-**2** products with an axial —CH_3 at the C_3 position, inducing an additional strain/deformation of the piperazine cycle in this latter case. The methyl groups preferring the equatorial position, it becomes obvious that the *exo* products are favored. Upon alkylation, because of sterical hindrance, the Boc moiety is reoriented *anti* to the newly bound methyl, again inducing strain in the piperazine cycle. The released chloride anion interacts with two hydrogen atoms from the 2-oxopiperazine as a consequence of stabilizing electrostatic interactions. The overall enol structures (the newly bound —CH_3 has not been considered) are now very different upon alkylation, as the rmsd between *exo* and *endo* configurations are now 1.36 Å and 1.15 Å for PostRC1 and PostRC2, respectively. It has to be acknowledged that the energy difference between the *exo* structures of PostRC1 and PostRC2 is 2.6 kcal mol^{-1} in favor of PostRC1 in the gas phase.

4.4. Discussion

The most relevant effect of the solvation is the stabilization of both the transition states and the post-reaction complexes, and in this latter case, the stabilization increases with the polarity of the solvent (Tables 2 and 3) because of a favorable solvation of the released chloride anion. The solvation does not change the *exo*/*endo* preferences but one can observe, especially for RP1, that the energy difference between the two enantiomers diminishes.

In RP1, from PreRC1 to TS1, there is a weakening of the HB-1 intramolecular hydrogen bond as its length increases from 1.75 Å to 1.82 Å in both attacks. As can be seen on Figs. 3 and SI3–5, the spacial arrangement of HB-1 impedes the incoming of the methyl chloride in the *endo* attack. In order to keep the intramolecular hydrogen bond distance at its optimal value while favoring the ingress of the methyl group, the system has to deform (bending/rotation of the alcohol function). The slightly higher deformation of the overall enol structure upon incoming of the *endo* MeCl is confirmed by the evaluation of the rmsd which is of 0.49 Å *vs.* 0.34 Å for the *exo* attack. Then from TS1 to PostRC1, the HB weakens again and now has a value of 1.93 Å and 1.90 Å for *exo* and *endo* products, respectively. Again, the overall deformation of the enol is

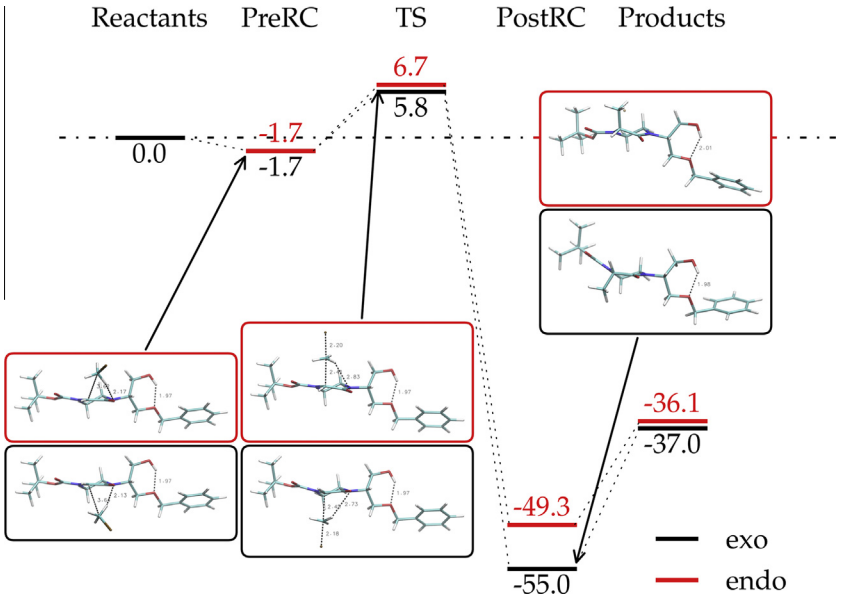

Fig. 4. Pre-reaction (PreRC), transition state (TS) and post-reaction (PostRC) structures for the *exo* and *endo* attacks of the HB-2 intramolecular hydrogen-bonded enolate of (1′R)-**1** by methyl chloride. The free energy differences between each state and the reactants are given in kcal mol^{-1}. Better quality images of the structures are given in Supplementary Information (SI6–9).

more important for the *endo* configuration (0.99 Å *vs.* 0.84 Å). The strong intramolecular hydrogen bonds in PreRC1 and TS1 locks the piperazine ring in its conformation, forcing its surroundings to deform and to adapt to the incoming methyl chloride. Upon alkylation and thus weakening of HB-1 because of the loss of the negative charge and subsequent equilibration of the electronic density, there is a release of the strain and the piperazine ring is able to deform in PostRC1. In RP2, compared to RP1, the intramolecular hydrogen bond is weaker by construction and its value does not vary much from PreRC2 to PostRC2 (see Figs. 4 and SI6–8), attesting of its non-participation in the alkylation process. Deformations of the enol structure are also less important than in the HB-1 case.

On the one hand, enols from 2-oxopiperazines featuring the intramolecular hydrogen bond pattern HB-1 are the most stable in the gas phase, but

(i) upon alkylation, they show more structural deformation, as HB-1 has to adapt to local sterical hindrance and a change of the electronic density on the carbonyl function along the reaction pathway;
(ii) in solution, the *exo*/*endo* preference is not as marked as in the gas phase.

On the other hand, enols from 2-oxopiperazines featuring the intramolecular hydrogen bond pattern HB-2 are less prone to form in the gas phase, but

(i) upon alkylation, the *exo*/*endo* preference is more significant than in the HB-1 case, especially when solvent is involved;
(ii) there is little deformation of the overall piperazine moiety throughout the reaction path.

As aforementioned, the most stable conformation for the 2-oxopiperazine reactant (1′*R*)-**1** possesses an intramolecular HB-2 pattern, so it could be possible for the system to swap from one pattern to another in order to minimize the energy losses upon reorganization/deformation.

In order to prove the validity of this initial model, we performed additional calculations using a lithium atom in place of the hydroxyl hydrogen for the pre-reaction, transition state and post-reaction structures in both the *exo* and *endo* approaches. We focused on the one conformation where the lithium bridges the two anionic oxygen atoms. Free energy differences obtained in the gas phase as well as in a solvent medium for the two reaction paths are given in Table 4. Detailed structures are given in Supplementary Information (Figs. SI9–11). Again, consistent with experimental results, the calculations favor the formation of the *exo* product by 4.7 kcal mol^{-1}. This energy difference is comparable to that obtained for RP1 and RP2.

Similarly, the geometrical results and observations for the structures featuring the lithium atom along the reaction path are comparable to those obtained for RP1, i.e., (i) the *endo* approach of the methyl chloride is impeded by the O···Li···O interaction and the axial hydrogen at position C_6, (ii) the transition state leading to the *exo* product is favored (by 1.6 kcal mol^{-1}) and (iii) deformations to accommodate the bonding of the methyl are observed. The main difference between this scheme and RP1 is the relative evolutions of the lengths of OLi···O and OH···O. In the previous scheme, the OH···O distance increases from PreRC1 to PostRC1, whereas in the new scheme the OLi···O distance remains constant.

Table 4
Free energy differences (in kcal mol^{-1}), at a temperature of 195 K and a pressure of 1 atm of Pre-Reaction complexes, Transition States and Post-Reaction complexes for RP-Li in the gas phase and in solution.

Solvent	Approach	Pre-RC	TS	Post-RC
Gas phase	*exo*	0.0	12.1	−38.6
	endo	1.3	13.7	−33.9
CCl_4	*exo*	0.0	8.9	−45.7
	endo	1.5	10.4	−42.4
$CHCl_3$	*exo*	0.9	6.2	−48.9
	endo	0.0	6.3	−46.3
THF	*exo*	0.0	6.1	−50.9
	endo	0.4	5.2	−49.4
n-Octanol	*exo*	0.4	5.5	−51.8
	endo	0.0	7.0	−50.2
Water	*exo*	0.3	6.7	−52.2
	endo	0.0	6.0	−51.8

Indeed, the predominantly ionic nature of the O···Li···O "bonds" allows a larger conformational freedom to the lithium ion between the two anionic sites. The consequences of these looser bonds are a less pronounced *exo*/*endo* preference (1.6 *vs.* 2.4 kcal mol^{-1} for TS and 4.7 *vs.* 5.0 kcal mol^{-1} for PostRC) and slightly reduced global deformations. Upon solvation, the *exo* preference is kept for the PostRC complexes; however, a gradual stabilization of the *endo* approach of the methyl can be seen to occur with increasing solvent polarities (except for *n*-octanol), eventually resulting in a switch to *endo* preference for THF and water (Table 4). The decomposition of the corresponding free energies into enthalpic and entropic terms (data not shown) reveals that this is due to the higher entropy of vibrational modes. At this point, we wish to stress that the vibrational frequencies of solvated systems are computed based on the minimized geometry of their gas-phase counterparts – an approximation which, although widely employed and usually correct [48], deteriorates with the increasing number of low-lying real frequencies. Indeed, not only does the RP-Li pathways present more modes below 50 cm^{-1} than RP1 (on average 30% more), but it also features more imaginary frequencies, which signifies that the gas-phase saddle point is a better approximation of the solvent one in the case of RP1 than RP-Li. When looking at the "raw" energies (see Tables SI1–3), the stabilization of *exo* over *endo* attacks in the transition states decreases with increasingly polar solvents (from 2 to 0.5 kcal mol^{-1} for RP1, and from 2 to 0.1 kcal mol^{-1} for RP-Li) – a fact we tentatively attribute to the progressive screening by the solvent of charge–charge interactions at different distances in both structures. Consequently, the error introduced by subsequent vibrational analyses (vibrational entropy, ZPE, ...) has a greater probability of flipping the order of the states' free energies in the case of polar solvents. In addition, the size of solvent molecules might not be adequately treated inside an implicit framework: this could explain that the polar but bulky *n*-octanol features a clear preference for *exo*-type transition states when comparing free energies (in contrast to water and THF), but this preference is much less marked when comparing energies. Clearly, the TS-Li systems, which feature both low-frequency vibrations and ions, push the limit of the chosen methodology [49] and would benefit from more realistic (but also much more costly) explicit-solvent calculations. This would also help to better characterize the apparent smaller preference for one attack over the other in polar solvents.

These additional calculations show that —OLi and —OH interact quite similarly with the nearby carbonyl function, which possesses a high electronic density. They provide validation of our simplified model and its *a priori* non-realistic reactive species (the non-deprotonated hydroxyl function). Modeling the reactant using a hydroxyl function and basing the discussion on hydrogen bonding patterns seems a relevant first approximation: this approach represents a good compromise between feasibility/limitations of the computational methods and the actual reaction occurring in the test tube; in particular, it avoids having to take into account aggregates formed by the lithium with its direct environment (THF solvent molecules) and prevents difficulties linked with the localization of the charge during the conformational search). The role of the chiral auxiliary, which was seen to induce rigidity and sterical hindrance *via* —OH/—OLi interactions, yields a first insight into one of the many complex mechanisms underlying this diastereoselective alkylation.

5. Conclusion

The computational results given in Table 1 unambiguously indicate a stereospecificity upon alkylation at position 3 of 2-oxopiperazines. Starting from a 1′*R* configuration, the resulting (1′*R*,3*S*) is always favored over the (1′*R*,3*R*) one, which is totally consistent with experimental results. The free energy difference between the most stable (1′*R*,3*S*) and (1′*R*,3*R*) structures is 1.8 kcal mol^{-1} at a temperature of −78 °C and a pressure of 1 atm, which corresponds to the experimental 98:2 ratio. From this result alone, the alkylation of 2-oxopiperazines would thus appear to be a thermodynamically driven reaction. However, the reaction paths leading to either the *endo* or the *exo* products and the energetics of the pre-reaction, post-reaction and transition state structures (Fig. 3) unambiguously prove that the alkylation of 2-oxopiperazines is a kinetically driven reaction. Even when considering distinct conformations of the reactants, the *exo* attack is always favored over the *endo* one, even for the least stable of the TS conformers. The selectivity does not depend on the conformation of the starting enol reactant, but the mechanisms driving this selectivity might differ with the conformation. Indeed, the presence of the Boc moiety and the alcohol chiral auxiliary blocks the conformation of the piperazine cycle thus impeding a ring inversion and subsequently favoring an approach of the electrophile where the methyl will be equatorially bound. Moreover, the presence of an intramolecular hydrogen bond, i.e., the formation of a pseudo 7-ring, between the alcohol function of the chiral auxiliary and the carbonyl function of the piperazine adds a new level of rigidity to the 2-oxopiperazine enol as well as sterical hindrance upon incoming of the methyl chloride, favoring the approach of the electrophile *anti* to the intramolecular hydrogen bond. These results confirm the early hypotheses of Micouin et al. on the origins of diastereoselectivity in the alkylation of *N*-substituted lactams [38].

In conclusion, apart from sterical hindrance in some selected conformations, there is no special effect of the substituent, as the C_3—C_M distance does not govern the stereoselectivity. The main source of the *exo* specificity upon alkylation is the imposed and controlled strain/rigidity of the piperazine ring imposed by the chiral auxiliary in the transition structure. Indeed, the preference for one conformation of this ring induces an enantiofacial selectivity upon approach of the electrophile.

Acknowledgements

The calculations presented in this work were performed using resources from the IDRIS facility (grant i2013087159) and the MeCS computing platform of Université de Picardie Jules Verne.

Appendix A. Supplementary material

Supplementary data associated with this article can be found, in the online version, at http://dx.doi.org/10.1016/j.comptc.2015.12.005.

References

[1] J.P. Vacca, B.D. Dorsey, W.A. Schleif, R.B. Levin, S.L. McDaniel, P.L. Darke, J. Zugay, J.C. Quintero, O.M. Blahy, E. Roth, L-735,524: an orally bioavailable human immunodeficiency virus type 1 protease inhibitor, Proc. Natl. Acad. Sci. U.S.A. 91 (1994) 4096–4100.
[2] R. Capdeville, E. Buchdunger, J. Zimmermann, A. Matter, Glivec (STI571, imatinib), a rationally developed, targeted anticancer drug, Nat. Rev. Drug Discov. 1 (2002) 493–502.
[3] S.E. Ward, P. Eddershaw, S.T. Flynn, L. Gordon, P.J. Lovell, S.H. Moore, C.M. Scott, P.W. Smith, K.M. Thewlis, P.A. Wyman, Studies on a series of potent, orally bioavailable, 5-HT(1) receptor ligands–Part II, Bioorg. Med. Chem. Lett. 19 (2009) 428–432.
[4] E.R. Ashley, E.G. Cruz, B.M. Stoltz, The total synthesis of (−)-lemonomycin, J. Am. Chem. Soc. 125 (2003) 15000–15001.
[5] M.L. Amador, J. Jimeno, L. Paz-Ares, H. Cortes-Funes, M. Hidalgo, Progress in the development and acquisition of anticancer agents from marine sources, Ann. Oncol. 14 (2003) 1607–1615.

[6] S. Nagumo, A. Matoba, Y. Ishii, S. Yamaguchi, N. Akutsu, H. Nishijima, A. Nishida, N. Kawahara, Synthesis of (−)-TAN1251A using 4-hydroxy-l-proline as a chiral source, Tetrahedron 58 (2002) 9871–9877.
[7] N.K. Garg, B.M. Stoltz, The formal total synthesis of dragmacidin B, trans-dragmacidin C, and cis- and trans-dihydrohamacanthins A, Tetrahedron Lett. 46 (2005) 2423–2426.
[8] H.J. Kim, W.Y. Kwak, J.P. Min, J.Y. Lee, T.H. Yoon, H.D. Kim, C.Y. Shin, M.K. Kim, S.H. Choi, H.S. Kim, E.K. Yang, Y.H. Cheong, Y.N. Chae, K.J. Park, J.M. Jang, S.J. Choi, M.H. Son, S.H. Kim, M. Yoo, B.J. Lee, Discovery of DA-1229: a potent, long acting dipeptidyl peptidase-4 inhibitor for the treatment of type 2 diabetes, Bioorg. Med. Chem. Lett. 21 (2011) 3809–3812.
[9] A. Khalaj, N. Adibpour, A.R. Shahverdi, M. Daneshtalab, Synthesis and antibacterial activity of 2-(4-substituted phenyl)-3(2H)-isothiazolones, Eur. J. Med. Chem. 39 (2004) 699–705.
[10] M.D. Arbo, M.L. Bastos, H.F. Carmo, Piperazine compounds as drugs of abuse, Drug Alcohol Depend. 122 (2012) 174–185.
[11] P. Kukula, R. Prins, Diastereoselective hydrogenation of pyrazine derivatives: an alternative method of preparing piperazine-(2S)-carboxylic acid, J. Catal. 208 (2002) 404–411.
[12] Z. Chen, A.S. Kende, A.O. Colson, J.L. Mendezandino, F.H. Ebetino, R.D. Bush, X.E. Hu, Ketopiperazines: conformationally constrained peptidomimetic of arginine amides, Synth. Commun. 36 (2006) 473–479.
[13] A. Viso, R.F. de la Pradilla, A. Flores, A. García, M. Tortosa, M.L. López-Rodríguez, Synthesis of highly substituted enantiopure piperazines and ketopiperazines from vicinal N-sulfinyl diamines, J. Org. Chem. 71 (2006) 1442–1448.
[14] G. Reginato, B. Di Credico, D. Andreotti, A. Mingardi, A. Paio, D. Donati, A new versatile and diastereoselective synthesis of polysubstituted 2-oxopiperazines from naturally occurring amino acids, Tetrahedron Asymmetry 18 (2007) 2680–2688.
[15] A. Pohlmann, V. Schanen, D. Guillaume, J.-C. Quirion, H.-P. Husson, Efficient Synthesis of conformationally constrained peptidomimetics containing 2-oxopiperazines 1, J. Org. Chem. 62 (1997) 1016–1022.
[16] V. Schanen, C. Riche, A. Chiaroni, J.-C. Quirion, H.-P. Husson, Asymmetric synthesis. XXXI. Synthesis of 2-substituted piperazines from chiral non-racemic lactams, Tetrahedron Lett. 35 (1994) 2533–2536.
[17] V. Schanen, M.-P. Cherrier, S.J. Melo, J.-C. Quirion, H.-P. Husson, Asymmetric synthesis; XXXVII: synthesis of 2,6-disubstituted piperazines from chiral non-racemic lactams, Synthesis 7 (1996).
[18] D. Hoppe, T. Hense, Enantioselective synthesis with lithium/(−)-sparteine carbanion pairs, Angew. Chem. Int. Ed. Engl. 36 (1997) 2282–2316.
[19] B.P. McDermott, A.D. Campbell, A. Ertan, First example of s-BuLi/(−)-sparteine-mediated chiral deprotonation of a piperazine and proof of the sense of induction, Synlett 6 (2008) 875–879.
[20] V. Santes, E. Gómez, V. Zárate, R. Santillan, N. Farfán, S. Rojas-Lima, Synthesis of new homochiral 2,3-dialkylpiperazines derived from (R)-(−)-phenylglycinol, Tetrahedron Asymmetry 12 (2001) 241–247.
[21] J. Seibel, D. Brown, A. Amour, S.J. Macdonald, N.J. Oldham, C.J. Schofield, Synthesis and evaluation of δ-lactams (piperazones) as elastase inhibitors, Bioorg. Med. Chem. Lett. 13 (2003) 387–389.
[22] J. DiMaio, B. Belleau, Synthesis of chiral piperazin-2-ones as model peptidomimetics, J. Chem. Soc. Perkin Trans. 1 (1989) 1687–1689.
[23] G.P. Pollini, N. Baricordi, S. Benetti, C. De Risi, V. Zanirato, A simple entry to chiral non-racemic 2-piperazinone derivatives, Tetrahedron Lett. 46 (2005) 3699–3701.
[24] C. De Risi, M. Pelà, G.P. Pollini, C. Trapella, V. Zanirato, Mastering chiral substituted 2-oxopiperazines, Tetrahedron Asymmetry 21 (2010) 255–274.
[25] D.C. Beshore, C.J. Dinsmore, Preparation of substituted piperazinones via tandem reductive amination-(N,N′-acyl transfer)-cyclization, Org. Lett. 4 (2002) 1201–1204.
[26] T. Prisinzano, K.C. Rice, M.H. Baumann, R.B. Rothman, Development of neurochemical normalization (“Agonist Substitution”) therapeutics for stimulant abuse: focus on the dopamine uptake inhibitor, GBR12909, Curr. Med. Chem.: Central Nerv. Syst. Agents 4 (2004) 47–59.
[27] A. Pohlmann, D. Guillaume, J.-C. Quirion, H.-P. Husson, Synthesis and conformational analysis of two 2-oxopiperazine-containing tetrapeptide analogues, J. Pept. Res. 51 (1998) 116–120.
[28] H. Kim, M.S. So, J. Chin, Preparation of chiral diamines by the diaza-Cope rearrangement (DCR), Aldrichim. Arta 41 (2008) 77–88.
[29] C.J. Carrano, K.N. Raymond, Coordination chemistry of microbial iron transport compounds. 10. Characterization of the complexes of rhodotorulic acid, a dihydroxamate siderophore, J. Am. Chem. Soc. 100 (1978) 5371–5374.
[30] G. Muller, B.F. Matzanke, K.N. Raymond, Iron transport in *Streptomyces pilosus* mediated by ferrichrome siderophores, rhodotorulic acid, and enantio-rhodotorulic acid, J. Bacteriol. 160 (1984) 313–318.
[31] B.F. Matzanke, G.I. Muller, K.N. Raymond, Hydroxamate siderophore mediated iron uptake in *E. coli*: stereospecific recognition of ferric rhodotorulic acid, Biochem. Biophys. Res. Commun. 121 (1984) 922–930.
[32] N. Franceschini, P. Sonnet, D. Guillaume, Simple, versatile and highly diastereoselective synthesis of 1,3,4-trisubstituted-2-oxopiperazine-containing peptidomimetic precursors, Org. Biomol. Chem. 3 (2005) 787–793.
[33] C. Leoneti, A. Lencina, P. Dassonville-Klimpt, Sonnet, New efficient enantioselective synthesis of 2-oxopiperazines: a practical access to chiral 3-substituted 2-oxopiperazines, Tetrahedron Asymmetry 19 (2008) 1689–1697.
[34] J.M. Um, N.S. Kaka, D.M. Hodgson, K.N. Houk, Transition states and origins of 1,4-asymmetric induction in alkylations of 2,2,6-trialkylpiperidine enamines, Chem. A: Eur. J. 16 (2010) 6310.
[35] H.K. Khartabil, P.C. Gros, Y. Fort, M.F. Ruiz-López, A theoretical study on nBuLi/lithium aminoalkoxide aggregation in hexane and THF, J. Org. Chem. 73 (2008) 9393–9402.
[36] W.F. Bailey, P. Beak, S.T. Kerrick, S. Ma, K.B. Wiberg, An experimental and computational investigation of the enantioselective deprotonation of Boc-piperidine, J. Am. Chem. Soc. 124 (2002) 1889–1896.
[37] I. Soteras, O. Lozano, A. Gomez-Esque, C. Escolano, M. Orozco, M. Amat, J. Bosch, F.J. Luque, On the origin of the stereoselectivity in the alkylation of oxazolopiperidone enolates, J. Am. Chem. Soc. 128 (2006) 6581–6588.
[38] L. Micouin, V. Jullian, J.-C. Quirion, H.-P. Husson, Origins of diastereoselectivity in the alkylation of N-substituted lactams and amides derived from optically active aminoalcohols, Tetrahedron Asymmetry 7 (1996) 2839–2846.
[39] R. Brückner, Chemistry of the alkaline earth metal enolates, in: H.A. Press (Ed.), Advanced Organic Chemistry: Reaction Mechanisms, 2002, pp. 373.
[40] H.J. Reich, Role of organolithium aggregates and mixed aggregates in organolithium mechanisms, Chem. Rev. 113 (2013) 7130–7178.
[41] Y. Ikuta, S. Tomoda, Origin of stereochemical reversal in Meyers-type enolate alkylations. Importance of intramolecular li coordination and solvent effects, Org. Lett. 6 (2004) 189–192.
[42] D. Romo, A.I. Meyers, Chiral non-racemic bicyclic lactams. Vehicles for the construction of natural and unnatural products containing quaternary carbon centers, Tetrahedron 47 (1991) 9503–9569.
[43] M.J. Frisch, G.W. Trucks, H.B. Schlegel, G.E. Scuseria, M.A. Robb, J.R. Cheeseman, G. Scalmani, V. Barone, B. Mennucci, G.A. Petersson, H. Nakatsuji, M. Caricato, X. Li, H.P. Hratchian, A.F. Izmaylov, J. Bloino, G. Zheng, J.L. Sonnenberg, M. Hada, M. Ehara, K. Toyota, R. Fukuda, J. Hasegawa, M. Ishida, T. Nakajima, Y. Honda, O. Kitao, H. Nakai, T. Vreven, J.A. Montgomery Jr., J.E. Peralta, F. Ogliaro, M.J. Bearpark, J. Heyd, E.N. Brothers, K.N. Kudin, V.N. Staroverov, R. Kobayashi, J. Normand, K. Raghavachari, A.P. Rendell, J.C. Burant, S.S. Iyengar, J. Tomasi, M. Cossi, N. Rega, N.J. Millam, M. Klene, J.E. Knox, J.B. Cross, V. Bakken, C. Adamo, J. Jaramillo, R. Gomperts, R.E. Stratmann, O. Yazyev, A.J. Austin, R. Cammi, C. Pomelli, J.W. Ochterski, R.L. Martin, K. Morokuma, V.G. Zakrzewski, G.A. Voth, P. Salvador, J.J. Dannenberg, S. Dapprich, A.D. Daniels, Ö. Farkas, J.B. Foresman, J.V. Ortiz, J. Cioslowski, D.J. Fox, Gaussian 09, Revision D.01, Gaussian Inc., Wallingford, CT, USA, 2009.
[44] A.D. Becke, Density-functional thermochemistry. III. The role of exact exchange, J. Chem. Phys. 98 (1993) 5648–5652.
[45] A.D. Becke, Density-functional exchange-energy approximation with correct asymptotic behavior, Phys. Rev. A 38 (1988) 3098–3100.
[46] C. Lee, W. Yang, R.G. Parr, Development of the Colle-Salvetti correlation-energy formula into a functional of the electron density, Phys. Rev. B: Condens. Matter 37 (1988) 785–789.
[47] T. Lu, F. Chen, Multiwfn: a multifunctional wavefunction analyzer, J. Comput. Chem. 33 (2012) 580–592.
[48] R.F. Ribeiro, A.V. Marenich, C.J. Cramer, D.G. Truhlar, Use of solution-phase vibrational frequencies in continuum models for the free energy of solvation, J. Phys. Chem. B 115 (2011) 14556–14562.
[49] J.H. Jensen, Predicting accurate absolute binding energies in aqueous solution: thermodynamic considerations for electronic structure methods, Phys. Chem. Chem. Phys. 17 (2015) 12441–12451.